ELSEVIER

Nuclear Physics A 628 (1998) 458–478

NUCLEAR PHYSICS A

Calculated nuclide production yields in relativistic collisions of fissile nuclei ★

J. Benlliure [a], A. Grewe [b], M. de Jong [b], K.-H. Schmidt [a], S. Zhdanov [c]

[a] *Gesellschaft für Schwerionenforschung, Planckstr. 1, 64291 Darmstadt, Germany*

[b] *Institut für Kernphysik, Schloßgartenstr. 9, 64289 Darmstadt, Germany*

[c] *Institute of Nuclear Physics, Alma Ata, Khasachstan*

Received 6 October 1997; accepted 20 October 1997

Abstract

A model calculation is presented which predicts the complex nuclide distribution resulting from peripheral relativistic heavy-ion collisions involving fissile nuclei. The model is based on a modern version of the abrasion-ablation model which describes the formation of excited prefragments due to the nuclear collisions and their consecutive decay. The competition between the evaporation of different light particles and fission is computed with an evaporation code which takes dissipative effects and the emission of intermediate-mass fragments into account. The nuclide distribution resulting from fission processes is treated by a semi-empirical description which includes the excitation-energy dependent influence of nuclear shell effects and pairing correlations. The calculations of collisions between ^{238}U and different reaction partners reveal that a huge number of isotopes of all elements up to uranium is produced. The complex nuclide distribution shows the characteristics of fragmentation, mass-asymmetric low-energy fission and mass-symmetric high-energy fission. The yields of the different components for different reaction partners are studied. Consequences for technical applications are discussed. © 1998 Elsevier Science B.V.

PACS: 25.75.-q; 25.85.-w; 24.10.-i; 24.10.Pa; 24.75.+i; 21.10.Ft; 21.10.Gv; 27.90.+b
Keywords: Relativistic heavy-ion collisions; Fission reactions; Semi-empirical nuclear-fission model; Predicted isotopic production yields

1. Introduction

Nuclide distributions after peripheral relativistic heavy-ion collisions have been studied for a long time, and it has been shown that the investigation of projectile fragmentation allows a complete identification of all fragments produced in the reaction (see e.g. Refs. [1,2]). Recently, heavier projectiles became available, and the investigations have

★ This work forms part of the Ph.D. thesis of A. Grewe.

PII S0375-9474(97)00607-6

been extended to the fragmentation of krypton [3,4], xenon [5,6] and gold [7]. Also radioactive beams with mass numbers around 60 have been applied [8,9]. These results have been compared to calculations in terms of the abrasion model [10–13] and of the intra-nuclear-cascade model [5,14]. In addition, they served to improve empirical systematics of fragmentation yields [15].

While all these measured nuclide distributions could be understood on a common basis involving the nuclear-collision process and the consecutive evaporation cascade, a direct comparison of the near-projectile fragment yields of ^{208}Pb and ^{238}U [16] clearly demonstrated the decisive influence of fission on the fragmentation process. On the other hand, the total fission cross section [17–19] as well as isotopic distributions of fission products [20] after relativistic nuclear collisions between ^{238}U and different reaction partners have been determined. Moreover, nuclear-charge distributions have been measured, using short-lived radioactive fissile projectiles [21,22]. These data revealed that also for very fissile nuclei most prefragments formed in the nuclear collision do not end up in fission but cool down by an evaporation cascade. This finding is in contrast to naive expectations since almost all prefragments are formed with excitation energies exceeding the fission threshold considerably. In a preceding paper, the influence of nuclear dissipation on the fission process according to the ideas of Kramers [23] and Grangé et al. [24] is quantitatively discussed [25] and shown to be responsible for a considerable suppression of the fission cross section after high-energetic nuclear collisions. In another study, the fission competition in excited spherical nuclei around neutron number 126 under the influence of shell effects and collective contributions to the level density has been determined [26]. With all these experimental data one has obtained a rather good information of the fission probabilities after fragmentation reactions.

The nuclide production yields of peripheral relativistic nuclear collisions are of considerable technical importance in several aspects. One application is the production of mass-separated radioactive nuclides in on-line mass separators [27] by bombarding heavy target materials with intense nuclear beams. These nuclides may also serve for the production of secondary beams by post acceleration [28–35]. In a similar application, however in inverse kinematics, a beam of about 1 AGeV ^{238}U has been used to produce mono-isotopic high-energetic secondary beams of projectile fragments and fission products at the fragment separator FRS at GSI [36,37].

Another field of interest which is presently discussed is the technical application of nuclear-collision processes for the energy production and the transmutation of nuclear waste in hybrid reactors [38,39] which work as a fission reactor where an additional high-energetic proton or ion beam serves to increase the neutron flux in the reactor in a controlled way. The desired neutron production is effected by a cascade of nuclear-collision processes in the region where the accelerated beam is fed into the reactor. However, in these collisions quite a number of nuclear species is produced. The recoil induced in the reaction as well as the expansion of gaseous products may damage the target material. Also the neutron-capture cross sections and the specific radioactive decay properties of the reaction products might be important for the operation of the reactor.

2. The model

2.1. The abrasion model

The initial stage of the nucleus–nucleus collision is considered as an abrasion process [10,11,40] in which the projectile is schematically divided into the overlapping "participant" and the non-overlapping "spectator" zone. Nucleons of the projectile and the target strongly interact in the overlapping zone while nucleons in the non-overlapping zone continue to move almost undisturbed with velocities close to the velocities of the projectile and the target, respectively. The mass of the spectators or prefragments is a function of the impact parameter. Their mean excitation energy of about 27 MeV per abraded particle is given by hole excitations and interactions with the hot participant zone [7,12]. Their neutron-to-proton ratio is subject to statistical fluctuations [8,12].

At larger impact parameters without nuclear contact, electromagnetic excitations are considered in accordance with the relations given in Refs. [41,42]. They are dominated by the isovector electric giant dipole resonance and lead to excitation energies close to the fission barrier.

2.2. The evaporation model

The second stage of the fragmentation reaction is treated in the framework of the statistical model. The emission probability of the particle j from the fragment with neutron number N, proton number Z and excitation energy E is determined by:

$$W_j(N,Z,E) = \frac{\Gamma_j(N,Z,E)}{\sum_k \Gamma_k(N,Z,E)}\,, \tag{1}$$

with j corresponding to the emitted particle and k denoting all possible decay channels.

Since the fragmentation process at relativistic energies is expected to populate low angular momenta [43] only, the particle emission width Γ_j can be approximated as [44]:

$$\Gamma_j = \frac{1}{2\pi\rho_c(E)}\frac{4m_jR^2}{\hbar^2}T_j^2\rho_j(E - S_j - B_j)\,, \tag{2}$$

where m_j is the particle mass, S_j the separation energy, B_j the effective Coulomb barrier in the case of charged particles [12]. ρ_c and ρ_j are the level densities of the compound nucleus and the exit channel, respectively. R is the radius of the nucleus and T_j the temperature of the residual nucleus after particle emission. The level densities were calculated by taking into account the influence of shell and pairing effects as described in Ref. [25]. The contribution of collective excitations to the level densities is considered, too. This topic is discussed in detail in a separate publication [26].

Since the model is intended to give predictions also for the production of lighter residues, the emission of intermediate-mass fragments (IMF) $3 \leqslant Z \leqslant 20$ is included in a simplified form as a sequential emission in the statistical model. In contrast to neutron and light charged particles ($Z \leqslant 2$) emission, the excitation of the IMFs is

included, and thus the emission widths Γ_j are calculated in the same way as for the light-particle emission, but the final level density ρ_j is calculated over the whole phase space of the final products as the convolution of the level densities of the residual nucleus and the emitted fragment by using the following expression:

$$\rho_j(E - S_j - B_j) = \iint \rho_1(E_1)\rho_2(E_2)\delta(E - S_j - B_j - E_1 - E_2)\, dE_1\, dE_2\,, \quad (3)$$

where the indices 1 and 2 refer to the residual nucleus and the emitted fragment, respectively.

The consecutive deexcitation of IMFs is included until the excitation energy of each residue falls below the lowest particle threshold.

2.3. The treatment of fission probabilities

The fission decay width in the statistical deexcitation has been included according to the transition-state method of Bohr and Wheeler [45] in the formulation of Ref. [44]:

$$\Gamma_f^{BW} = \frac{1}{2\pi\rho_c(E)} T_f\, \rho_f(E - B_f)\,, \quad (4)$$

where ρ_f is the level density of transition states in the fissioning nucleus in the saddle-point configuration. B_f is the height of the fission barrier and T_f the corresponding nuclear temperature.

The influence of nuclear viscosity on the fission width is included as deduced from experimental data [25], using the reduced friction coefficient with the value $\beta = 1 \times 10^{21}$ s^{-1}. The reduction of the fission width due to nuclear viscosity was applied according to the description given in Ref. [25].

2.4. A semi-empirical model of the fission-fragment properties

The fission decay channel, especially at low excitation energy, is a very complicated process which is far from being fully understood. The influence of nuclear structure on the fission process manifests itself most evidently in the observed mass distributions. A large body of experimental information has been accumulated on mass distributions of many fissioning systems at low excitation energies where the influence of nuclear structure is strong. There exist rather elaborate models for the description of nuclear fission (e.g. Refs. [46–50]) which are able to reproduce measured fission-fragment isotopic distributions in specific cases with considerable success. However, these calculations are complex and very time consuming, and the predictive power for regions where no experimental data exist is not known. Some models even use parameters which are individually adjusted to the experimental distributions of each system. Therefore, we decided to develop a semi-empirical description of the nuclide distributions produced in the fission process. The semi-empirical description of the fission process presented in the following has some similarities with previously published approaches, e.g. Refs. [51,52]. How-

ever, in contrast to those we intend to describe the fission properties of a large number of fissioning nuclei in a wide range of excitation energies.

On the one hand, it was tried to follow some basic ideas of existing theoretical models in order to assure a certain predictive power. On the other hand, special weight was attributed to reproduce global trends of the large body of experimental information. The model should be able to predict the magnitudes and widths of mass-symmetric and mass-asymmetric components, the even–odd fluctuations and the neutron-to-proton ratio of the fission-fragment distributions as a function of nuclear charge, mass and excitation energy of the fissioning nucleus in a global way. Since ^{238}U was chosen as a reaction partner in the model calculations presented below, special care was taken that the model well reproduces the low-energy fission yields of nuclei in the vicinity of ^{238}U.

First, we would like to give a short overview on the actual understanding of nuclear fission for orientation. The yields of the fission fragments are determined by the dynamic evolution of the system from the saddle to the scission point, see e.g. Ref. [50]. Since a full calculation of the dynamic path is not available, some simplified guidelines have been proposed. Scission-point models ([46,53]) describe the properties of fission fragments by the properties of the scission-point configuration, based on the assumption of a total or partial thermal equilibrium of the degrees of freedom at the scission point. In the concept of fission channels, however, a decisive influence of the potential-energy landscape between saddle and scission is assumed. Separate components in the yields and in the total kinetic energies of the fission fragments, called fission channels, are identified with fission paths along valleys in the potential energy of the highly deformed fissioning system in the direction of elongation [49,50]. The strongest channels showing up in the fission of most actinides are two mass-asymmetric ones producing fragments around the neutron numbers 82 and 88, and a mass-symmetric one. Calculations of the potential-energy landscape within the shell correction method, predict two minima in the potential energy at the fission barrier as a function of mass asymmetry, one leading to symmetric fission and a second one leading to asymmetric fission [50]. Slightly beyond the fission barrier, the asymmetric fission valley is predicted to bifurcate into two valleys, one leading to fission fragments with neutron number around $N = 82$ and one leading to fragments with neutron numbers around $N = 88$. Clear evidence has been obtained for the existence of different thresholds for symmetric and asymmetric fission components [54–56], thus demonstrating the influence of the properties of the saddle-point configuration on the fission-fragment distributions. Even the competition of different fission components as a function of the excitation energy has successfully been explained by the temperature dependence of shell effects in the statistical weight of transition states at the fission barrier [56,57]. This seems to indicate, that the population of the fission valleys is determined rather early, long before reaching the scission configuration.

In the approach formulated by Brosa et al. [50], the weights of the different channels are treated as free parameters to be determined by experiment. The valleys in the potential-energy surface down to the scission configuration are extracted from shell correction calculations. They determine the positions of the channels in mass number.

Finally, at the scission configuration, fluctuations in the mass split are induced by the random-neck rupture.

As an essential extension to this approach, we developed a description of the population probability of the different fission valleys. This was necessary to predict fission-fragment distributions for nuclei which have not yet been investigated. The potential-energy surface is treated in a simplified, semi-empirical way replacing a shell correction calculation. Fluctuations in the mass-asymmetry degree of freedom on the way from barrier to scission are taken into account empirically in the final widths of the mass distributions. This empirical description replaces the random-neck-rupture approach of Brosa et al. or possible influence of dynamics effects at the descent stage.

The population of the fission channels is assumed to be basically determined by the statistical weight of transition states above the potential-energy landscape near the fission barrier. As an approximation, the shape of the potential energy at the barrier as a function of mass-asymmetry was modeled in a way to reproduce the measured characteristics of fission-fragment distributions. As just mentioned, this simplification does not completely coincide with present theoretical calculations of the deformation potential energy landscapes [49,50], but it enables an easy way for a quantitative computation.

In the following we assume that the mass-asymmetric degree of freedom at the fission barrier is on average uniquely related to the neutron number N of the fission fragments. The numbers of protons and neutrons are considered to be strictly correlated (the small fluctuation in the charge density will be introduced later). Thus, we will express the mass-asymmetric deformation at the fission barrier by the corresponding number of neutrons N in one of the preformed fragments.

For a given excitation energy E, the yield $Y(E,N)$ of fission fragments with neutron number N is calculated by the statistical weight of transition states above the conditional potential barrier:

$$Y(E,N) = \frac{\int_0^{E-V(N)} \rho_N(U)\,dU}{\sum_{N=0}^{N_{CN}} \int_0^{E-V(N)} \rho_N(U)\,dU}, \tag{5}$$

where $V(N)$ is the height of the conditional potential barrier for a given mass-asymmetric deformation, ρ_N is the level density for an energy U above this potential and N_{CN} is the neutron number of the fissioning nucleus.

In accordance with experimental results, we define three main components of the potential at the fission barrier as a function of mass-asymmetric deformation. The first is the symmetric (V_{mac}) component defined by the liquid-drop description by means of a parabolic function. This parabola is assumed to be modulated by two neutron shells, located at mass asymmetries corresponding to the neutron numbers $N = 82$ ($V_{sh,1}$) and around $N = 88$ ($V_{sh,2}$) in the nascent fragments. The shell effects are represented by Gaussians as a function of the mass asymmetry. ($N = 82$ is known in literature as

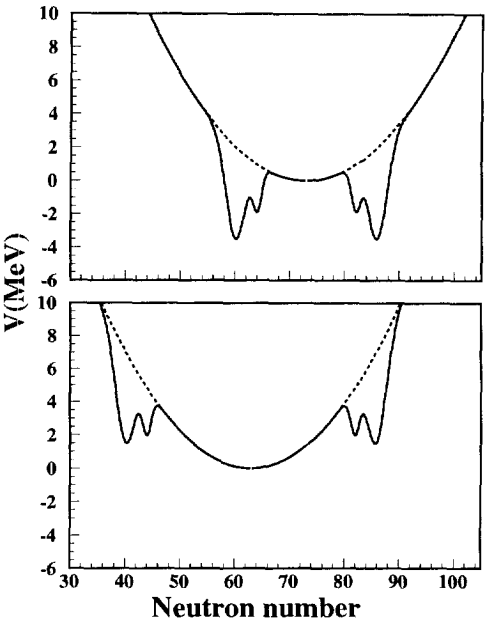

Fig. 1. Potential energy at the fission barrier for ^{238}U (upper part) and ^{208}Pb (lower part), as a function of mass asymmetry expressed by the neutron number of one of the preformed fragments.

standard I, $N \approx 88$ as standard II.) The influence of shell effects in the light fragments and any shell effects in proton number are neglected. The total potential energy at the fission barrier is thus given by the sum of five contributions:

$$\begin{aligned} V(N) = & V_{\mathrm{mac}}(N) \\ & + V_{\mathrm{sh},1}(N) + V_{\mathrm{sh},1}(N_{\mathrm{CN}} - N) \\ & + V_{\mathrm{sh},2}(N) + V_{\mathrm{sh},2}(N_{\mathrm{CN}} - N) \,. \end{aligned} \tag{6}$$

Note that the potential energy is symmetric around $N_{\mathrm{CN}}/2$.

The macroscopic part of the potential energy at the fission barrier as a function of the mass-asymmetry degree of freedom has been taken from experiment [58]. It has been deduced from the widths of measured mass distributions at higher excitation energies. The macroscopic potential energy (V_{mac}) at the fission barrier is formulated as:

$$V_{\mathrm{mac}}(N) = C_{\mathrm{mac}}(N - N_{\mathrm{CN}}/2)^2 \,, \tag{7}$$

where the curvature ($2C_{\mathrm{mac}}$) of the parabola was obtained by fitting the data points given in Ref. [58] to the expression:

$$C_{\mathrm{mac}} = \frac{8}{N_{\mathrm{CN}}^2} \frac{d^2 V_{\mathrm{mac}}}{d\eta^2} \,, \tag{8}$$

Table 1
Parameters for shell structures which best describe the experimental data

Shell position ($N_{sh,i}$)	Strength (δU_i) (MeV)	Curvature ($2\,C_{sh,i}$) (MeV)
82	−2.5	1.4
86–90	−5.5	0.16

$$\frac{d^2V_{mac}}{d\eta^2} = \begin{cases} 30.544 - 4.002\frac{Z_{CN}^2}{A_{CN}} + 0.120\left(\frac{Z_{CN}^2}{A_{CN}}\right)^2 \text{ MeV} & 25 < \frac{Z_{CN}^2}{A_{CN}} < 33.15\,, \\ 10^{7.16993 - 0.26602\frac{Z_{CN}^2}{A_{CN}} + 0.00283\left(\frac{Z_{CN}^2}{A_{CN}}\right)^2} \text{ MeV} & \frac{Z_{CN}^2}{A_{CN}} \geqslant 33.15\,, \end{cases} \tag{9}$$

where

$$\eta = \frac{4}{A_{CN}}\left(A - \frac{A_{CN}}{2}\right),$$

with A_{CN} the mass of the fissioning nucleus and A the mass of the fission fragment.

Fig. 1 demonstrates the potential energy at the fission barrier for two nuclei, ^{208}Pb and ^{238}U. From these examples we might conclude a general tendency, the absolute depth of the potential at the different shells which determines the yields is influenced rather strongly by the magnitude of the macroscopic part of the potential: shells which appear near symmetry are supported, others are weakened by the macroscopic potential. This explains a systematic trend in the appearance of different fission channels as a function of the neutron number and proton number of the fissioning nucleus.

In order to simplify the calculations we can approximate the shell-correction Gaussians in the vicinity of their respective minima by parabolic functions with curvatures $2C_{sh,1}$ and $2C_{sh,2}$. These curvature values were deduced from the widths of the standard I and the standard II components in the measured mass distribution of ^{213}At fission fragments [59]. In the case of this rather light nucleus one expects that fission barrier and scission point almost coincide, so that the presently proposed fission model should reproduce the fission-fragment mass distribution without considering any broadening on the way from the fission barrier to scission (see below). The parameters of the two parabolas which best describe the experimental yields are listed in Table 1.

Yields of fission fragments with neutron number N corresponding to the different fission channels can be obtained from the expressions:

$$Y_{mac}(E_0^*, N) \approx \exp\left(2\sqrt{\tilde{a}\,E_{mac}(E_0^*, N)}\right), \tag{10}$$

$$Y_{sh,i}(E_0^*, N) \approx \exp\left(2\sqrt{\tilde{a}\,E_{sh,i}(E_0^*, N)}\right) - Y_{mac}(E_0^*, N)\,, \tag{11}$$

where E_0^* is the excitation energy above the macroscopic potential at symmetry ($N_{CN}/2$) and Y_{mac} stands for the symmetric channel and $Y_{sh,i}$ for one of the asymmetric channels.

In Eq. (11) the contribution of the symmetric channel is subtracted in order to avoid double counting. The asymptotic level-density parameter is calculated as $\tilde{a} = A/8$.

The effective excitation energies above the macroscopic potential (E_{mac}) and above the shell-corrected potential ($E_{\mathrm{sh},i}$) to be inserted in Eqs. (10) and (11) are calculated as:

$$E_{\mathrm{mac}}(E_0^*, N) = E_0^* - C_{\mathrm{mac}}(N_{\mathrm{CN}}/2 - N)^2 , \tag{12}$$

$$E_{\mathrm{sh},i}(E_0^*, N) = E_{\mathrm{mac}}(E_0^*, N) - \delta U_i(E_0^*, N) . \tag{13}$$

In these expressions $\delta U_i(E_0^*, N)$ is the value of the shell-correction-parabolic function parametrized in Table 1. The energy dependence of this shell correction is described according to the analytical description of Ref. [60].

$$\delta U_i(E_0^*, N) = (\delta U_i + C_{\mathrm{sh},i}(N_{\mathrm{sh},i} - N)^2) \exp(-\gamma\epsilon) . \tag{14}$$

The factor γ is calculated as $\tilde{a}/(0.4A_{\mathrm{CN}}^{4/3})$ as proposed in Ref. [61] and $\epsilon = E_{\mathrm{mac}} + C_{\mathrm{sh},i}(N_{\mathrm{sh},i} - N)^2 + \delta U_i$.

Expanding expressions (10) and (11), we obtain in a first approximation that the neutron-dependent statistical weight of each fission channel can be expressed as a Gaussian function:

$$Y_{\mathrm{mac}}(E_0^*, N) \approx \exp(S_{\mathrm{mac}}) \exp\left(\frac{-(N_{\mathrm{CN}}/2 - N)^2}{\sigma_{\mathrm{mac}}^2}\right) , \tag{15}$$

$$Y_{\mathrm{sh},i}(E_0^*, N) \approx \exp(S_{\mathrm{sh},i}) \exp\left(\frac{-(N_{\mathrm{sh},i} - N)^2}{\sigma_{\mathrm{sh},i}^2}\right) - Y_{\mathrm{mac}}(E_0^*, N) , \tag{16}$$

with

$$S_{\mathrm{mac}} = 2\sqrt{\tilde{a}E_0^*} , \tag{17}$$

$$S_{\mathrm{sh},i} = 2\sqrt{\tilde{a}[E_{\mathrm{mac}}(E_0^*, N) - \delta U_i(E_0^*, N)]} , \tag{18}$$

and the widths of these Gaussian functions are given by:

$$\sigma_{\mathrm{mac}}^2 = \frac{1}{2}\frac{\sqrt{E_0^*}}{\sqrt{\tilde{a}}C_{\mathrm{mac}}} , \tag{19}$$

$$\sigma_{\mathrm{sh},i}^2 = \frac{1}{2}\frac{\sqrt{E_{\mathrm{mac}}(E_0^*, N) - \delta U_i(E_0^*, N)}}{\sqrt{\tilde{a}}C_{\mathrm{sh},i} \exp(-\gamma\epsilon)} . \tag{20}$$

From this calculation we obtain three components of the mass distributions: The first is the macroscopic contribution which is symmetric and rather broad. Its width is given by the expression (19). The eventual broadening of this component on the way from the fission barrier to scission is neglected because the width calculated with the curvature of the potential at the fission barrier was directly deduced from experimental mass-yield data. The second and third contributions are the asymmetric components in the vicinity of $N = 82$ and $N \approx 88$, respectively. Guided by experimental results [62], the widths

(Eq. (20)) are assumed to be increased on the way from the fission barrier to scission. The final width is formulated in the following way:

$$\sigma^2_{\mathrm{sh},1} = 21 \qquad \text{for} \quad Z^2/A \geqslant 35\,, \tag{21}$$

for the component at $N = 82$ and

$$\sigma^2_{\mathrm{sh},2} = 14\left(\frac{Z^2_{\mathrm{CN}}}{A_{\mathrm{CN}}} - 33\right)\,, \tag{22}$$

for the component near $N \approx 88$. Relations (21) and (22) which are fitted to data points given in Ref. [62] are taken if their values exceeds those of Eq. (20).

The neutron-to-proton ratio is assumed to be given by the unchanged charge density (UCD) of the fissioning nucleus. For the asymmetric channels, a polarization of $|\Delta Z| = 0.5$ is included to approximately reproduce the measured neutron-to-proton ratio [63,64].

$$Z(N) = N\frac{Z_{\mathrm{CN}}}{N_{\mathrm{CN}}} \pm \Delta Z\,, \tag{23}$$

where the different signs correspond to the light (+) and the heavy (−) fragment. The width in proton number for fixed neutron number $\sigma_{Z|N}$ is calculated by using the following formula:

$$\sigma^2_{Z|N} = \frac{1}{2}\frac{\sqrt{E_{\mathrm{mac}}(E^*_0, N)}}{\sqrt{\tilde{a}}C_{Z|N}} + \sigma^2_0\,, \tag{24}$$

where the term $\sigma_0 = 0.4$ is used to take into account the influence of quantum fluctuations [63] not considered in the statistical picture, and the curvature $2C_{Z|N}$ is calculated in a touching-sphere configuration for a symmetric split as:

$$C_{Z|N} = \left.\frac{d^2V}{dZ^2}\right|_N = B(Z+1,N) + B(Z-1,N) - 2B(Z,N) - \frac{e^2}{r_0^2}\left[\frac{(Z+1)(Z-1)}{(A+1)^{1/3}+(A-1)^{1/3}} - \frac{Z^2}{2A^{1/3}}\right]\,, \tag{25}$$

with e the electron charge, $r_0 = 1.22$ fm the radius parameter and $\mathrm{B}(Z,N)$ representing the macroscopic binding energy of a nucleus with Z protons and N neutrons. The element yields are modulated by an even–odd effect formulated following Ref. [65], where the variation of this effect with the fissility parameter is given by:

$$\delta_p = \exp\left(29.86 - 0.74Z^2_{\mathrm{CN}}/A_{\mathrm{CN}}\right)\,, \tag{26}$$

and the energy dependence is obtained as:

$$\delta_p(E) = \begin{cases} \delta_p & 0 \leqslant E \leqslant E_1\,, \\ \delta_p \exp\left(-\dfrac{E-E_1}{T}\right) & E > E_1\,, \end{cases} \tag{27}$$

where $T = 1$ MeV and $E_1 = V_{\mathrm{B}} + 2\Delta$, with V_{B} the height of the fission saddle point and Δ the pairing gap calculated as $\Delta = 12/\sqrt{A_{\mathrm{CN}}}$.

The part of post-scission neutron emission due to the deformation of the fission products and its evolution with the excitation energy was taken into account. The mean post-scission neutron number $\nu(A)$ due to deformation was obtained as a parametrization of data taken from Ref. [66]. Consecutive evaporation from the excited fission fragments is included, too. The excitation energy of the fragments is taken as the sum of the excitation energy above the barrier and the intrinsic excitation energy E_{dis} on the way from the fission barrier to scission. The latter is parametrized in the following way [67]:

$$E_{\mathrm{dis}} = 3.53(Z_{\mathrm{CN}}^2/A_{\mathrm{CN}} - 34.25)\,. \tag{28}$$

The final excitation energy is attributed to the fission fragments proportionally to their mass values.

Fig. 2 shows the comparison of experimental and calculated mass distributions for some cases. The solid lines correspond to predictions obtained with the proposed model and the dashed lines represent the same calculations but including post-scission neutron emission. In the left column we present the mass distributions of fission products obtained for the reaction n+^{235}U at different energies, data were taken from Ref. [68]. In general we obtain a good description of the experimental data with our calculation, in particular we are able to reproduce the competition between the different fission components as a function of the excitation energy of the fissioning nucleus.

In the right column we observe also the evolution of the fission components for different fissioning nuclei [69–71]. In order to improve the agreement with the experimental data, the position of the deformed neutron shell $N \approx 88$ was shifted between $N = 86$ and $N = 90$ when the mass of the fissioning nucleus decreases. In this case we obtain also a good description of the data with our calculation. In these calculations the structures caused by the two neutron shells included in the present description are clearly seen. We also observe the appearance of post-scission neutron emission at higher excitation energies. In Fig. 3 we compare our calculations with experimental charge distributions of two different nuclei taken from Ref. [68,72]. The general trends of these distributions are well reproduced, including the even–odd effect.

Although the model is restricted to a few rather schematic features, it is able to describe many of the most prominent characteristics of measured fission-fragment mass and charge distributions. In particular, the variation of the strengths of the different fission channels over a large region of nuclei (Ra–Pu) is reproduced, including the appearance of multi-modal fission in pre-actinides.

2.5. *Kinematical description*

The fragmentation process induces momentum fluctuations in beam direction ($\sigma_{\parallel}$) and perpendicular to it ($\sigma_{\perp}$) combined with an average longitudinal momentum shift ($P_{\parallel}$). In the rest frame of the projectile, these quantities can be described by the empirical systematics proposed by Morrissey [73] as a function of the mass difference (ΔA) between the projectile and the fragment:

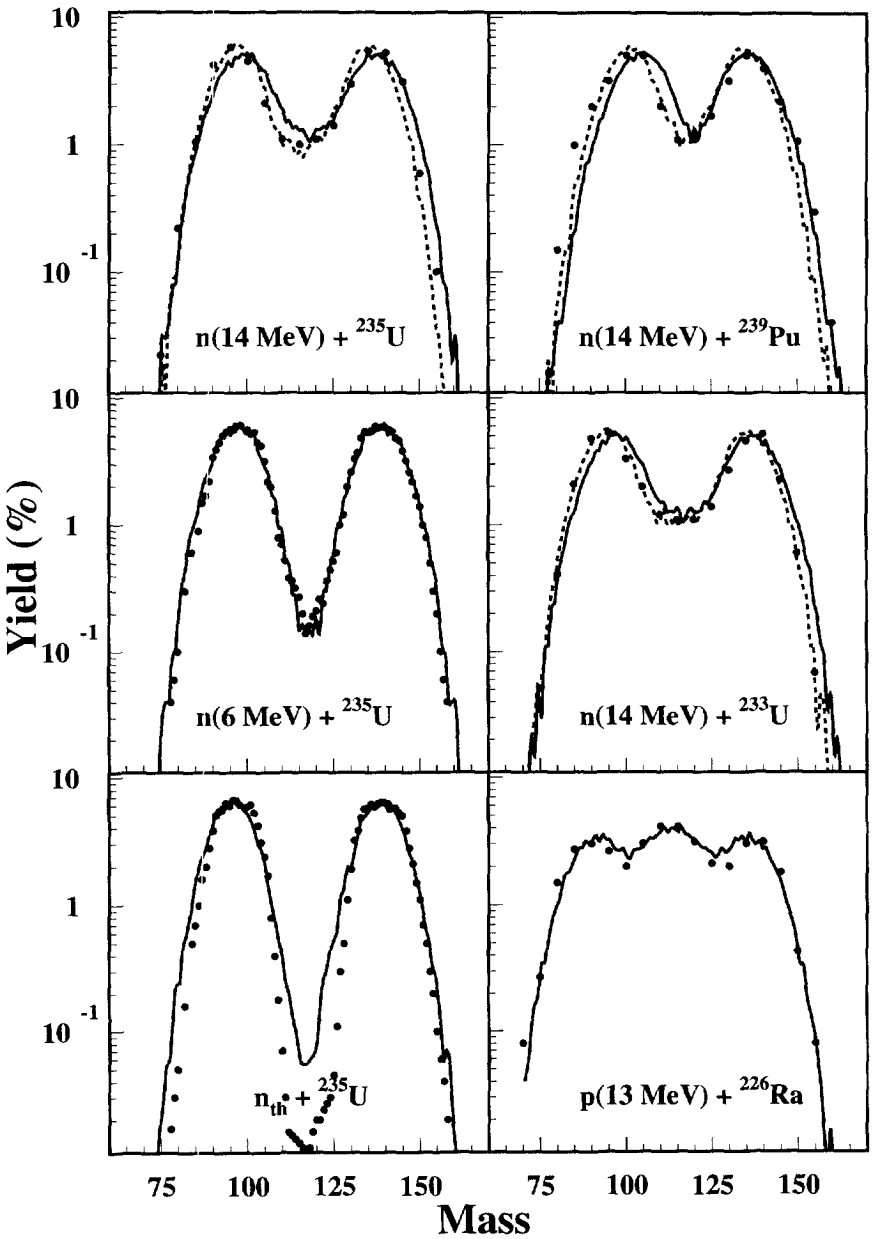

Fig. 2. Comparison for experimental (full points) and calculated (lines) mass distributions. The solid lines correspond to the result obtained with the proposed model and the dashed lines represent the same calculation but including post-scission neutron evaporation. The position of the second neutron shell was set to 90 for radium, to 89 for uranium and to 86 for plutonium.

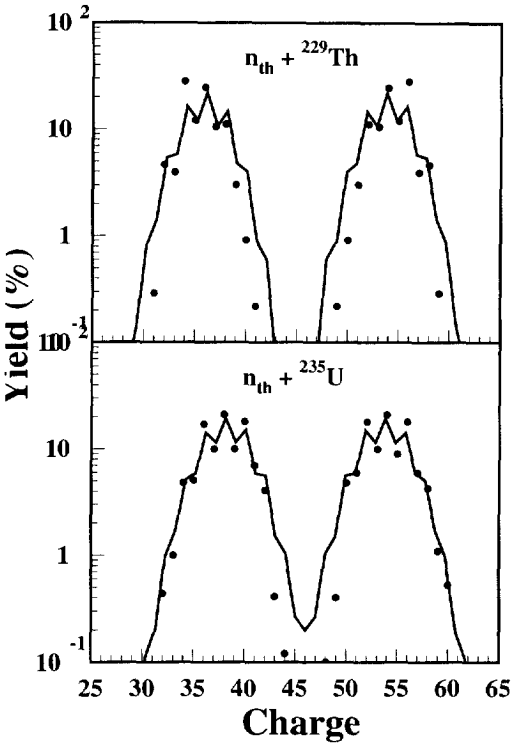

Fig. 3. Comparison between experimental (full points) and calculated (lines) fission charge distributions. The position of the second neutron shell was set to 89 in both cases.

$$\sigma_{\parallel} \approx \sigma_{\perp} = 87\sqrt{\Delta A}\ \mathrm{MeV}/c\,, \tag{29}$$

$$P_{\parallel} = -8\Delta A\ \mathrm{MeV}/c\,. \tag{30}$$

The root-mean-squared momentum of the fragmentation products is given by:

$$\langle P_{\mathrm{rms}}\rangle^{1/2} = \sqrt{\sigma_{\parallel}^2 + \sigma_{\perp}^2 + P_{\parallel}^2}\,. \tag{31}$$

The kinematical properties of fission fragments can be obtained by the liquid-drop-model systematics given by Wilkins et al. [46]:

$$E_c = \frac{e^2 Z_1 Z_2}{R_1 + R_2 + 2\ \mathrm{fm}}\,. \tag{32}$$

The major semiaxes of both fission fragments can be obtained as:

$$R_i = r_0 A^{1/3}\left(1 + \frac{2\beta}{3}\right)\,, \tag{33}$$

where $r_0 = 1.16$ fm and the deformation parameter $\beta = 0.625$ are taken from Ref. [46].

In Fig. 5 we represent the evolution of the root-mean-squared velocity of fragmentation (solid line) and fission (dashed line) residues in the frame of the projectile, as a function

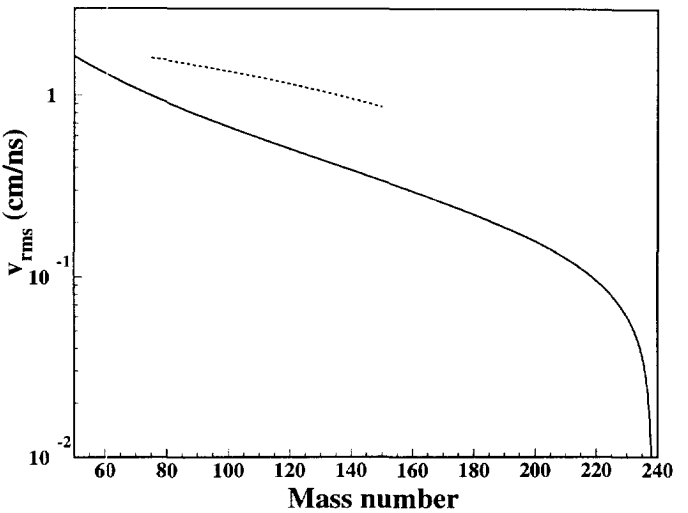

Fig. 4. Root-mean-squared velocity of fragmentation (solid line) and fission (dashed line) residues in the frame of the projectile, produced in the reaction U(1 *A* GeV)+Pb as a function of its mass.

of its mass. Note that the root-mean-squared velocities are essentially independent of the target material, since they primarily result from the Fermi momentum of the nucleons in the case of fragmentation and from Coulomb repulsion of the fission fragments in the case of fission.

3. Results and discussion

A complete calculation with this model allows us to predict the complex nuclide distribution resulting from peripheral relativistic heavy-ion collisions. In order to illustrate the different reaction mechanisms contributing to these distributions we have performed calculations with a uranium projectile at 1 *A* GeV with different targets.

In Fig. 5 we report on a chart of nuclides the isotopic distributions of all the residues produced in the reactions ^{238}U(1 *A* GeV)+Pb (upper part) and ^{238}U(1 *A* GeV)+Be (lower part). In these pictures, the color scale and the size of the clusters give the production cross section of each isotope. In both cases we observe the production of very neutron-rich isotopes by means of the asymmetric fission of the projectile. As we explained in Section 2.2, this asymmetric fission is produced by the electromagnetic excitation of the projectile at large impact parameters without nuclear contact. This Coulomb excitation is proportional to the squared charge of the target, which explains the higher production cross sections for this process that we obtain with the lead target if compared to the beryllium target. Coulomb excitation also leads to high abundances of the one- and two-neutron-removal channels.

In very peripheral reactions, a low excited projectile spectator is produced which deexcites by means of the competition between neutron or proton evaporation and

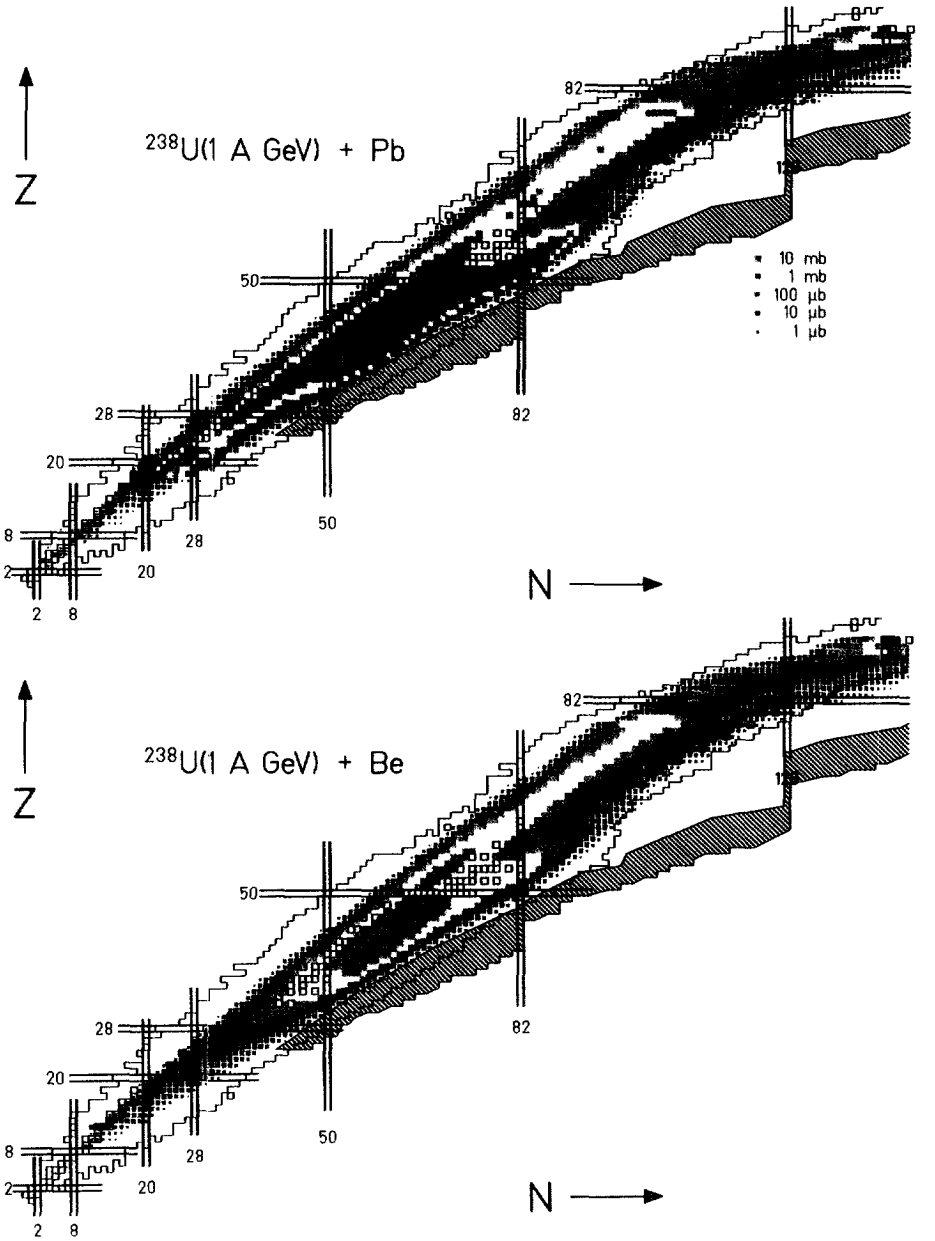

Fig. 5. Calculated isotopic distributions of all the residues produced in the reaction ^{238}U(1 *A* GeV)+Pb (upper part) and ^{238}U(1 *A* GeV)+Be (lower part). The cross sections are represented by the size and the color of the clusters. The color scale is given in the upper figure. The outer contour line includes the known isotopes. The black hatched area indicates the nuclei involved in the stellar r-process [74].

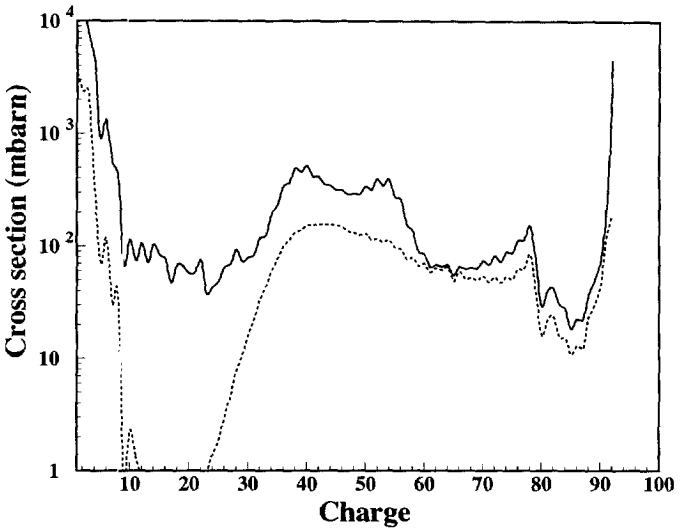

Fig. 6. Calculated production cross section of the different elements produced with a uranium beam at 1 *A* GeV and different targets: Pb (solid line) and Be (dashed line).

fission. The value of the nuclear viscosity defines the ratio between particle evaporation and fission, especially at excitation energies larger than 100 MeV, as shown in Ref. [25]. All the isotopes close to the projectile in charge and mass are populated by the neutron or proton evaporation channel. The higher excitation energies involved in these reactions lead to symmetric fission as can be observed in both pictures.

At lower impact parameter, the size of the projectile spectator decreases and its excitation energy increases. Under these conditions, the deexcitation mechanism is dominated by the emission of light particles. The neutron excess of the projectile and the Coulomb barrier produce a shift to the neutron-deficient isotopes on the chart of the nuclides. At higher excitation energies, the evaporation of intermediate-mass fragments plays a not negligible role. In this way, the evaporation-residue corridor is populated.

The production cross sections of isotopes along this evaporation-residue corridor depends on the amount of energy dissipated in the reaction and, in the scenario of an abrasion model, on the size of the reaction partners. To illustrate this effect, in Fig. 6 we compare the production cross sections of the different elements produced with both targets, lead (solid line) and beryllium (dashed line).

In the low-energy regime ($Z \geqslant 30$) the production of fragmentation residues is comparable with both targets. In the fission region ($30 \leqslant Z \leqslant 60$), the increase of the electromagnetic excitation with the charge of the target induces a larger production of asymmetric fission residues with the lead target. The region of lighter residues is also very differently populated with both targets. In fact, within our model the amount of energy dissipated in the reaction depends on the size of the partners and the impact parameter, this explains that this charge interval ($Z < 30$) corresponds to strongly dissipative reactions leading to very high excitation energies which are easily attained with

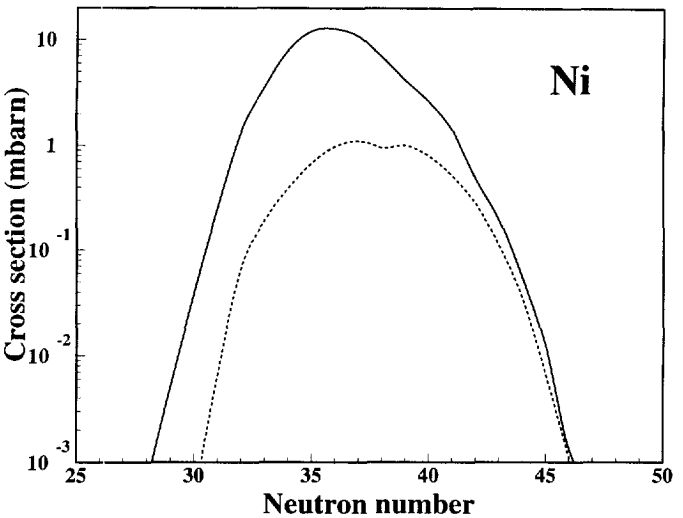

Fig. 7. Calculated production cross section of nickel isotopes with a uranium beam and different targets: U(1 AGeV)+Pb (solid line) and U(1 AGeV)+Be (dashed line).

a heavy target (Pb) rather than with a light one (Be). The increase of the production cross sections of very light fragments ($Z < 10$) is a consequence of the evaporation process. Once more the higher excitation energies attained with the lead target explain the more abundant intermediate-mass fragment emission with this target.

The predictions of the present model closely compare to experimental results on production cross sections in reactions with relativistic ^{238}U projectiles obtained in recent experiments [16,75–77]. A quantitative comparison with a detailed discussion of these data will be performed elsewhere.

One of the main interests of this kind of calculations is its predictive power for the production of exotic nuclei. Reactions with heavy ions at relativistic energies allow to produce neutron-rich or neutron-deficient isotopes by means of fission or fragmentation reactions, respectively. The nuclei with predicted production cross sections exceeding 1 μb reach the limits of known isotopes in many cases. Especially for heavy elements which are not produced by fission, it seems to be possible to reach a number of new isotopes on both extremes, the neutron-rich and the neutron-deficient side, by fragmentation reactions. For elements up to about xenon the production yields extend into the region of isotopes which are involved in the stellar r-process of nucleosynthesis. Thus, new results on relevant decay properties of these nuclei are expected from future secondary-beam experiments.

In the region of neutron-rich fission fragments, a considerable effort has been made to extend the limits of known isotopes [78]. Here the most neutron-rich isotopes have been produced in the reaction ^{238}U+Be at 750 AMeV with cross sections around 1 nb. This is in agreement with extrapolations of the present calculation.

The choice of the projectile and the target will define the final production yield of each isotope. In order to illustrate these effects, in Fig. 7 we compare the production cross

section of nickel isotopes obtained with a uranium beam at 1 A GeV and two different targets, beryllium and lead. As we discussed before, the neutron-deficient isotopes are mainly populated by fragmentation reactions with a lead target. In contrast, neutron-rich isotopes are produced in fission reactions. In this case, the nickel isotopes are mainly populated by nuclear fission reactions rather than by electromagnetic fission; in fact we observe nearly the same production cross section with both targets. In this case the final production yields will be determined by the number of atoms in the target.

4. Conclusion

The description of the fragmentation of fissile nuclei requires to consider many different processes. Large impact parameters without nuclear contact lead to electromagnetic excitations with cross sections depending on the charge of the reaction partner. Electromagnetic excitations lead to a loss of a few neutrons or to low-energy fission. With decreasing impact parameter, the nuclei come into contact, and the violence of the collision increases gradually, leading to increasing loss of nucleons and growing excitation energies. Mostly neutron-deficient fragmentation products and fragments of hot fission are resulting from these reactions. In addition, neutrons, protons and intermediate-mass fragments are formed due to the high excitation energies induced in the nuclear collision.

In the present work, a semi-empirical model for the fission process has been developed which covers a broad range in nuclear composition and excitation energy of the fissioning system. By combining this model with several approaches available in literature for the other processes involved, a complete description of the fragmentation process of fissile nuclei could be obtained.

Corresponding to the different reaction mechanisms involved, the products have very different recoil velocities, ranging from the very low values of electromagnetic dissociation products over the recoil of the fragmentation products given by the Fermi momentum of the abraded particles to the kinetic energies of the fission fragments given by the Coulomb repulsion and the high velocities of the emitted nucleons and light nuclei.

Thus, any technical application of the fragmentation involving fissile nuclei has to face a complex situation where different elements and even different isotopes of the same element may be produced with very different characteristics.

These characteristics are relevant for the intensities of secondary beams either due to their formation cross sections or due to their kinematic properties. Another important implication is the production of specific elements or isotopes in hybrid reactors. Besides the yields of gaseous elements and isotopes with specific radioactive properties, here the recoil velocities are particularly important for possible radiation damages.

References

[1] T.J.M. Symons, Y.P. Yiyogi, G.D. Westfall, P. Doll, D.E. Greiner, H. Faraggi, P.J. Lindstrom, H.J. Crawford, C. McParland, Phys. Rev. Lett. 42 (1979) 40.

[2] G.D. Westfall, T.J.M. Symons, D.E. Greiner, H.H. Heckman, P.J. Lindstrom, J. Mahoney, A.C. Shotter, D.K. Scott, H.J. Crawford, C. McParland, T.C. Awes, C.K. Gelbke, J.M. Kidd, Phys. Rev. Lett. 43 (1979) 1859.
[3] C. Stéphan, L. Tassan-Got, D. Bachelier, C.O. Bacri, R. Rimbot, B. Boderie, J.L. Boyard, F. Clapier, C. Donzaud, T. Hennino, M.F. Rivet, P. Roussel, D. Bazin, C. Grunberg, D. Disdier, B. Lott, Phys. Lett. B 262 (1991) 6.
[4] M. Weber, C. Donzaud, J.-P. Dufour, H. Geissel, A. Grewe, D. Guillemaud-Müller, H. Keller, M. Lewitowicz, A. Magel, A. C. Müller, G. Münzenberg, F. Nickel, M. Pfützner, A. Piechaczek, M. Pravikoff, E. Roeckl, K. Rykacyewski, M.G. Saint-Laurent, I. Schall, C. Stéphan, K. Sümmerer, L. Tassan-Got, D.J. Vieira, B. Voss, Nucl. Phys. A 578 (1994) 659.
[5] K.-H. Schmidt, K. Sümmerer, H. Geissel, G. Münzenberg, F. Nickel, M. Pfützner, M. Weber, B. Voss, T. Brohm, H.-G. Clerc, M. Fauerbach, J.-J. Gaimard, A. Grewe, E. Hanelt, M. Steiner, J. Weckenmann, C. Ziegler, A. Magel, Nucl. Phys. A 452 (1992) 699.
[6] J. Friese, H.-J. Körner, J. Reinhold, R. Schneider, H. Trieb, K. Zeitelhack, B. Blank, T. Brohm, Y. Fujita, H. Geissel, W. König, G. Münzenberg, F. Nickel, M. Pfützner, K. Rykaczewski, I. Schall, D. Schardt, A. Schröter, M. Steiner, K. Sümmerer, B. Voss, J. Weckenmann, Nucl. Phys. A 553 (1993) 753c.
[7] K.-H. Schmidt, T. Brohm, H.-G. Clerc, M. Dornik, M. Fauerbach, H. Geissel, A. Grewe, E. Hanelt, A. Junghans, A. Magel, W. Morawek, G. Münzenberg, F. Nickel, M. Pfützner, C. Scheidenberger, K. Sümmerer, D. Vieira, B. Voss, C. Ziegler, Phys. Lett. B 300 (1993) 313.
[8] Th. Brohm, K.-H. Schmidt, Nucl. Phys. A 569 (1994) 821.
[9] M. Pfützner, S. Andriamonje, B. Blank, R. Del Moral, J.P. Dufour, A. Fleury, T. Josso, M.S. Pravikoff, T. Brohm, A. Grewe, E. Hanelt, A. Heinz, A. Junghans, C. Röhl, S. Steinhäuser, B. Voss, K.-H. Schmidt, S. Czajkowski, Z. Janas, A. Piechaczek, E. Roeckl, K. Sümmerer, W. Trinder, M. Weber, M. Fauerbach, Nucl. Phys. A 587 (1995) 229.
[10] Y. Eisenberg, Phys. Rev. 96 (1954) 1378.
[11] J.D. Bowman, W.J. Swiatecki, C.E. Tsang, report LBL 2908, unpublished, 1973.
[12] J.-J. Gaimard, K.-H. Schmidt, Nucl. Phys. A 531 (1991) 709.
[13] T. Brohm, H.-G. Clerc, M. Dornik, M. Fauerbach, J.-J. Gaimard, A. Grewe, E. Hanelt, B. Voss, Ch. Ziegler, B. Blank, R. Del Moral, J.-P. Dufour, L. Faux, C. Marchand, M.S. Pravikoff, K.-H. Schmidt, H. Geissel, G. Münzenberg, F. Nickel, M. Pfützner, E. Roeckl, I. Schall, K. Sümmerer, D.J. Vieira, M. Weber, Nucl. Phys. A 550 (1992) 540.
[14] Y. Yariv, Z. Fraenkel, Phys. Rev. C 20 (1979) 2227.
[15] K. Sümmerer, W. Brüchle, D.J. Morrissey, M. Schädel, B. Szweryn, Yang Weifan, Phys. Rev. C 42 (1990) 2546.
[16] H.-G. Clerc, M. de Jong, T. Brohm, M. Dornik, A. Grewe, E. Hanelt, A. Heinz, A. Junghans, C. Röhl, S. Steinhäuser, B. Voss, C. Ziegler, K.-H. Schmidt, S. Czajkowski, H. Geissel, H. Irnich, A. Magel, G. Münzenberg, F. Nickel, A. Piechacyek, C. Scheidenberger, W. Schwab, K. Sümmerer, W. Trinder, M. Pfützner, B. Blank, A.V. Ignatyuk, G.A. Kudyaev, Nucl. Phys. A 590 (1995) 785.
[17] Th. Rubehn, W.F.J. Müller, R. Bassini, M. Begemann-Blaich, Th. Blaich, A. Ferrero, C. Gross, G. Imme, I. Iori, G.J. Kunde, W.D. Kunze, V. Lindenstruth, U. Lynen, T. Möhlenkamp, L.G. Moretto, B. Ocker, J. Pochodzalla, G. Raciti, S. Reito, H. Sann, A. Schüttauf, W. Seidel, V. Serfling, W. Trautmann, A. Trzcinski, G. Verde, A. Wörner, E. Zude, B. Zwieglinski, Z. Physik A 353 (1995) 197.
[18] P. Armbruster, M. Bernas, S. Czajkowski, H. Geissel, T. Aumann, Ph. Dessagne, C. Donzaud, E. Hanelt, A. Heinz, M. Hesse, C. Kozhuharov, Ch. Miehe, G. Münzenberg, M. Pfützner, K.-H. Schmidt, W. Schwab, C. Stéphan, K. Sümmerer, L. Tassan-Got, B. Voss, Z. Phys. A 355 (1996) 191.
[19] M. Hesse, M. Bernas, P. Armbruster, T. Aumann, S. Czajkowski, Ph. Dessagne, C. Donzaud, H. Geissel, E. Hanelt, A. Heinz, C. Kozhuharov, Ch. Miehe, G. Münzenberg, M. Pfützner, C. Röhl, K.-H. Schmidt, W. Schwab, C. Stéphan, K. Sümmerer, L. Tassan-Got, Z. Phys. A 355 (1996) 69.
[20] M. Bernas, S. Czajkowski, P. Armbruster, H. Geissel, P. Dessagne, C. Donzaud, H.-R. Faust, E. Hanelt, A. Heinz, M. Hesse, C. Kozhuharov, Ch. Miehe, G. Münzenberg, M. Pfützner, C. Röhl, K.-H. Schmidt, W. Schwab, C. Stéphan, K. Sümmerer, L. Tassan-Got, B. Voss, Phys. Lett. B 331 (1994) 19.
[21] K.-H. Schmidt, A. Heinz, H.-G. Clerc, B. Blank, T. Brohm, S. Czajkowski, C. Donzaud, H. Geissel, E. Hanelt, H. Irnich, M.C. Itkis, M. de Jong, A. Junghans, A. Magel, G. Münzenberg, F. Nickel, M. Pfützner, A. Piechaczek, C. Röhl, C. Scheidenberger, W. Schwab, S. Steinhäuser, K. Sümmerer, W. Trinder, B. Voss, S.V. Zhdanov, Phys. Lett. B 325 (1994) 313.

[22] C. Böckstiegel, S. Steinhäuser, J. Benlliure, H.-G. Clerc, A. Grewe, A. Heinz, M. de Jong, A.R. Junghans, J. Müller, K.-H. Schmidt, Phys. Lett. B 398 (1997) 259.
[23] H.A. Kramers, Physica 7 (1940) 284.
[24] P. Grangé, L. Jun-Qing, H.A. Weidenmüller, Phys. Rev. C 27 (1983) 2063.
[25] A.V. Ignatyuk, G.A. Kudyaev, A. Junghans, M. de Jong, H.-G. Clerc, K.-H. Schmidt, Nucl. Phys. A 593 (1995) 519.
[26] A.R. Junghans, M. de Jong, H.-G. Clerc, A.V. Ignatyuk, G.A. Kudyaev, K.-H. Schmidt, Nucl. Phys. A, to be published.
[27] H.L. Ravn, Nucl. Instr. and Meth. B 26 (1987) 72.
[28] D. Guerreau, Proc. of the Int. Workshop on Gross Properties of Nuclei and Nuclear Excitations. Hirschegg, Austria, January 1996.
[29] D. Habs, O. Kester, K. Rudolph, P. Thirolf, G. Hinderer, E. Nolte, G. Bollen, H. Raimbault-Hartmann, H. Ravn, F. Ames, L. Liljeby, K.G. Rensfelt, D. Schwalm, R. von Hahn, R. Repnow, A. Schempp, U. Ratzinger, P. Van Duppen, M. Huyse, G. Walter, Nucl. Instr. and Meth. B 126 (1996) 218.
[30] I. Tanihata, Nucl. Instr. and Meth. B 126 (1996) 224.
[31] P.G. Bricault, M. Dombsky, P.W. Schmor, G. Stanford, Nucl. Instr. and Meth. B 126 (1996) 231.
[32] A.M. Rodin, S.I. Sidorchuk, S.V. Stepantsov, G.M. Ter-Akopian, A.S. Fomichev, R. Wolski, V.B. Galinskiy, G.N. Ivanov, I.B. Ivanova, V.A. Gorshkov, A.Yu. Lavrentyev, Yu.Ts. Oganessian, Nucl. Instr. and Meth. B 126 (1996) 236.
[33] G. Ciavola, L. Calabretta, G. Cuttone, G. Di Bartolo, P. Finocchiaro, S. Gammino, M. Gu, E. Migneco, J. Qin, G. Raia, D. Rifuggiato, A. Rovelli, D. Vinciguerra, H. Wollnik, Nucl. Instr. and Meth. B 126 (1996) 258.
[34] J.A. Pinston, Nucl. Instr. and Meth. B 126 (1996) 22.
[35] P. Van Duppen, P. Decrock, M. Huyse, Th. Delbar, W. Galster, P. Leleux, I. Licot, E. Liénard, P. Lipnik, M. Loiselet, C. Michotte, G. Ryckewaert, J. Vervier, P. Duhamel, J. Vanhorenbeeck, Nucl. Instr. and Meth. B 70 (1992) 393.
[36] A. Magel, H. Geissel, B. Voss, P. Armbruster, T. Aumann, M. Bernas, B. Blank, T. Brohm, H.-G. Clerc, S. Czajkowski, H. Folger, A. Grewe, E. Hanelt, A. Heinz, H. Irnich, M. de Jong, A. Junghans, F. Nickel, M. Pfützner, A. Piechaczek, C. Röhl, C. Scheidenberger, K.-H. Schmidt, W. Schwab, S. Steinhäuser, K. Sümmerer, W. Trinder, H. Wollnik, G. Münzenberg, Nucl. Instr. and Meth. B 94 (1994) 548.
[37] Ch. Engelmann, F. Ameil, P. Armbruster, M. Bernas, S. Czajkowski, Ph. Dessagne, C. Donzaud, H. Geissel, A. Heinz, Z. Janas, C. Koshuharov, Ch. Miehe, G. Münzenberg, M. Pfützner, C. Röhl, W. Schwab, C. Stéphan, K. Sümmerer, L. Tassan-Got, B. Voss, Z. Phys. A 352 (1995) 351.
[38] C.D. Bowman, E.D. Arthur, P.W. Lisowski, G.P. Lawrence, R.J. Jensen, J.L. Anderson, B. Blind, M. Cappiello, J.W. Davidson, T.R. England, L.N. Engel, R.C. Haight, H.G. Hughes III, J.R. Ireland, R.A. Krakowski, R.J. LaBauve, B.C. Letellier, R.T. Perry, G.J. Russell, K.P. Staudhammer, G. Versamis, W.B. Wilson, Nucl. Instr. and Meth. A 320 (1992) 336.
[39] C. Rubbia, CERN report CERN-LHC-96-011-EET.
[40] J. Hüfner, K. Schäfer, B. Schürmann, Phys. Rev. C 12 (1975) 1888.
[41] C.A. Bertulani, G. Baur, Phys. Rep. 163 (1988) 299.
[42] A. Grewe, S. Andrianonje, C. Böckstiegel, T. Brohm, H.-G. Clerc, S. Czajkowski, E. Hanelt, A. Heinz, M.G. Itkis, M. de Jong, A. Junghans, M.S. Pravikoff, K.-H. Schmidt, S. Steinhäuser, K. Sümmerer, B. Voss, Nucl. Phys. A 614 (1997) 400.
[43] M. de Jong, A.V. Ignatyuk, K.-H. Schmidt, Nucl. Phys. A 613 (1997) 435.
[44] L.G. Moretto, Proc. third IAEA Symp. on the physics, chemistry of fission, Rochester, NY, 13-17 August 1973, vol. 1 (IAEA, Vienna, 1974) p. 329.
[45] N. Bohr, J.A. Wheeler, Phys. Rev. 56 (1939) 426.
[46] B.D. Wilkins, E.P. Steinberg, R.R. Chasman, Phys. Rev. C 14 (1976) 1832.
[47] J.W. Negele, S.E. Koonin, P. Möller, J.R. Nix, A.J. Sierk, Phys. Rev. C 17 (1978) 1098.
[48] J.F. Berger, M. Girod, D. Gogny, Nucl. Phys. A 428 (1984) 23.
[49] V.V. Pashkievich, Nucl. Phys. A 169 (1971) 275.
[50] U. Brosa, S. Grossmann, A. Müller, Phys. Rep. 197 (1990) 167.
[51] M.G. Itkis, S.I. Mulgin, A. Ya. Rusanov, A.N. Okolovich, G.N. Smirenkin, Yad. Fiz. 43 (1986) 1125 (Sov. J. Nucl. Phys. 43 (1986) 719).
[52] P.P. Jauho, A. Jokinen, M. Leino, J.M. Parmonen, H. Penttilä, J. Äystö, K. Eskola, V.A. Rubchenya, Phys. Rev. C 49 (1994) 2036.

[53] P. Fong, Phys. Rev. 102 (1956) 434.
[54] R. Konecny, H.J. Specht, J. Weber in Proc. Third Symp. Phys. Chem. Fission IAEA, Vol. 2, Vienna, 1974, p. 3.
[55] J. Weber, J.C. Britt, A. Gavron, E. Konecny, J. B. Wilhemly, Phys. Rev. C 13 (1976) 2413.
[56] G.A. Kudyaev, Yu.B. Ostapenko, B, N. Smirenkin, Yad. Fiz. 45 (1987) 1534 (Sov. J. Nucl. Phys. 45 (1987) 951).
[57] G.A. Kudyaev, Yu.B. Ostapenko, E.M. Rastopchin, Yad. Fiz. 47 (1988) 1540 (Sov. J. Nucl. Phys. 47 (1988) 976).
[58] M.G. Itkis, V.N. Okolovich, A.Ya. Rusanov, G.N. Smirekin, Fiz. Elem. Chastits At. Yadra 19 (1988) 701 (Sov. J. Part. Nucl. 19 (1988) 301).
[59] E.N. Gruzintsev, M.G. Itkis, Yu.V. Kotlov, V.N. Okolovich, A.Ya. Rusanov, G.N. Smirenkin, Yad. Fiz. 47 (1988) 1201 (Sov. Journ. Nucl. Phys. 47 (1988) 765).
[60] A.V. Ignatyuk, K.K. Istekov, G.N. Smirekin, Yad. Fiz. 29 (1979) 875 (Sov. J. Nucl. Phys. 29 (1979) 450).
[61] K.-H. Schmidt, H. Delagrange, J.P. Dufour, N. Carjan, A. Fleury, Z. Phys. A 308 (1982) 215.
[62] S.D. Beizin, S.V. Zhdanov, M.G. Itkis, V.N. Okolovich, G.N. Smirenkin, Yad. Fiz. 53 (1991) 656 (Sov. J. Nucl. Phys. 53 (1991) 411).
[63] W. Lang, H.-G. Clerc, H. Wohlfarth, H. Schrader, K.-H. Schmidt, Nucl. Phys. A 345 (1980) 34.
[64] A.C. Wahl, At. Data Nucl. Data Tables 39 (1988) 1.
[65] S. Pommé, E. Jacobs. K. Persyn, D. De Frenne, K. Govaert, M.-L. Yoneama, Nucl. Phys. A 560 (1993) 689.
[66] C.J. Bishop, R. Vandenbosch, R. Aley, R.W. Shaw, J. Halpern Nucl. Phys. A 150 (1970) 129.
[67] B.D. Wilkins et al., Proc. Int. Symp. Nucl. Fission, Heavy Ion Induced Reactions, W. Schröder, ed. Harwood 1986.
[68] Ch. Sträde, C. Butz-Jorgensen, H.-H. Knitter, Nucl. Phys. A 462 (1987) 129.
[69] D.G. Perry, A.W. Fairhall, Phys. Rev. C 4 (1971) 977.
[70] E.A.C. Crouch, At. Nucl. Data Table 19 (1977) 418.
[71] J.E. Gindler, L.E. Glendenin, D.J. Henderson, J.W. Meadows, Phys. Rev. C 27 (1983) 2058.
[72] M. Djebara, M. Asghar, J.P. Bocquet, R. Brissot, M. Maurel, H. Nifenecker, Ch. Ristori, Nucl. Phys. A 425 (1984) 120.
[73] D.J. Morrissey, Phys. Rev. C 39 (1989) 460.
[74] K.L. Kratz, private comunication.
[75] J. Benlliure, P. Armbruster, M. Bernas, C. Böckstiegel, S. Czajkowski, P. Dessagne, C. Donzaud, H. Geissel, A. Heinz, C. Kozhuharov, Ch. Miehe, G. Münzenberg, M. Pfützner, K.-H. Schmidt, C. Stéphan, K. Sümmerer, L. Tassan-Got, B. Voss, submitted to Z. Phys. A.
[76] C. Donzaud, S. Czajkowski, P. Armbruster, M. Bernas, C. Böckstiegel, P. Dessagne, H. Geissel, E. Hanelt, A. Heinz, C. Kozhuharov, Ch. Miehe, G. Münzenberg, M. Pfützner, W. Schwab, C. Stéphan, K. Sümmerer, L. Tassan-Got, B. Voss, submitted to Z. Phys. A.
[77] W. Schwab, M. Bernas, P. Armbruster, T. Aumann, S. Czajkowski, P. Dessagne, C. Donzaud, H. Geissel, E. Hanelt, A. Heinz, C. Kozhuharov, Ch. Miehe, G. Münzenberg, M. Pfützner, K.-H. Schmidt, C. Stéphan, K. Sümmerer, L. Tassan-Got, B. Voss, in preparation.
[78] M. Bernas, C. Engelmann, P. Armbruster, S. Czajkowski, F. Ameil, C. Böckstiegel, P. Dessagne, C. Donzaud, H. Geissel, A. Heinz, Z. Janas, C. Kozhuharov, Ch. Miehe, G. Münzenberg, M. Pfützner, W. Schwab, C. Stéphan, K. Sümmerer, L. Tassan-Got, B. Voss, Phys. Lett. B., to be published.